A Comprehensive Review of Axial-Flux Permanent-Magnet Machines
Revue de littérature sur les machines à aimant permanent à flux axiale

Solmaz Kahourzade, *Student Member, IEEE*, Amin Mahmoudi, *Member, IEEE*, Hew Wooi Ping, *Member, IEEE*, and Mohammad Nasir Uddin, *Senior Member, IEEE*

***Abstract*— This paper presents a state-of-the-art review of axial-flux permanent-magnet (AFPM) machines in the aspects of construction, features, electromagnetic and thermal modeling, simulation, analysis, design, materials, and manufacturing. Some key references on the above-mentioned aspects pertaining to the machine are discussed briefly. Particular emphasis is given on the design and performance analysis of AFPM machines. A comparison among different permanent magnet machines is also provided. Thus, this paper makes a bridge between the currently used permanent magnet machines in industry and the recent developments of AFPM machines.**

***Résumé*— Cet article présente une revue sur l'état de l'art de la construction, caractéristiques, modélisation thermique et électromagnétique, simulation, analyse, conception et matériaux des machines à aimant permanent à flux axiale (APFA). Quelques références importantes portant sur les aspects mentionnés ci-dessus des machines sont abordées brièvement. La conception et l'analyse des performances des machines APFA sont présentées avec plus de détails. Une comparaison entre les différentes machines à aimant permanent est également présentée. Ainsi, ce papier est une jonction entre les machines à aimant permanent actuellement utilisés dans l'industrie et les développements récents des machines APFA.**

***Index Terms*— Axial-flux permanent-magnet machine (AFPM), cogging torque, design, field weakening, finite-element analysis, generator, motor, optimization.**

I. Introduction

THE development of axial-flux permanent-magnet (AFPM) machines has been slow compared to that of conventional radial-flux permanent-magnet (RFPM) machines because of the lack of fabrication technology of AFPM machines. This limitation results from the strong axial magnetic attraction between the stator and rotor, which causes the deflection of rotor discs and fabrication difficulties such as lamination in the slotted stator, high cost, and assembly [1]. However, the higher torque-to-weight ratio due to the application of less core material, smaller size, planar and easily adjustable air gap, lower noise, and lower vibration make AFPM machines superior to RFPM machines [2]. Before Davenport claimed the first patent for the radial-flux machine in 1837 [3], the axial-flux machine was invented by Faraday in 1831 as the first electrical machine [4]. The AFPM machines have been widely used in numerous applications, from domestic to high-industrial and military applications, renewable energy systems to transportation, wherever extreme axial compactness coupled with high torque density and high efficiency are necessary. The AFPM machine topologies have been extensively investigated. However, despite the significant development in the AFPM machine technology, a gap still exists in industrial applications and some key aspects in the analysis and design of such machines published in recent papers. Therefore, this paper presents a comprehensive review on the analysis, design, and prototyping of AFPM machines.

Manuscript received October 21, 2013; revised January 7, 2014; accepted February 11, 2014. Date of current version May 6, 2014. This work was supported by the University of Malaya under the High Impact Research Grant D000022-16001 which funds the Hybrid Solar Energy Research Suitable for Rural Electrification.

S. Kahourzade, A. Mahmoudi, and H. W. Ping are with the UM Power Energy Dedicated Advanced Centre, Wisma Research and Development UM, University of Malaya, Kuala Lumpur 59990, Malaysia (e-mail: solmazkahourzade@gmail.com; amaminmahmoudi@gmail.com; wphew@um.edu.my).

M. N. Uddin is with the Department of Electrical Engineering, Lakehead University, Thunder Bay, ON P7B 5E1, Canada (e-mail: muddin@lakeheadu.ca).

Associate Editor managing this paper's review: S. R. Samantaray.

Color versions of one or more of the figures in this paper are available online at http://ieeexplore.ieee.org.

Digital Object Identifier 10.1109/CJECE.2014.2309322

II. AFPM Machines Topologies

The AFPM machine structure includes surface mounted or interior PMs, with or without armature slots, with or without armature core, with ring winding or drum winding, and single- or multistage. Fig. 1 shows various topologies of AFPM machines. The AFPM machines are classified as single-stator single-rotor (SSSR), single-stator double-rotor (SSDR), double-stator single-rotor (DSSR), or multistator multirotor (MSMR). All mentioned design configurations are briefly described as follows.

A. SSSR Machine

The simplest structure of the AFPM machine is single-stator single-rotor (SSSR) [5]. Fig. 2 depicts an example of SSSR

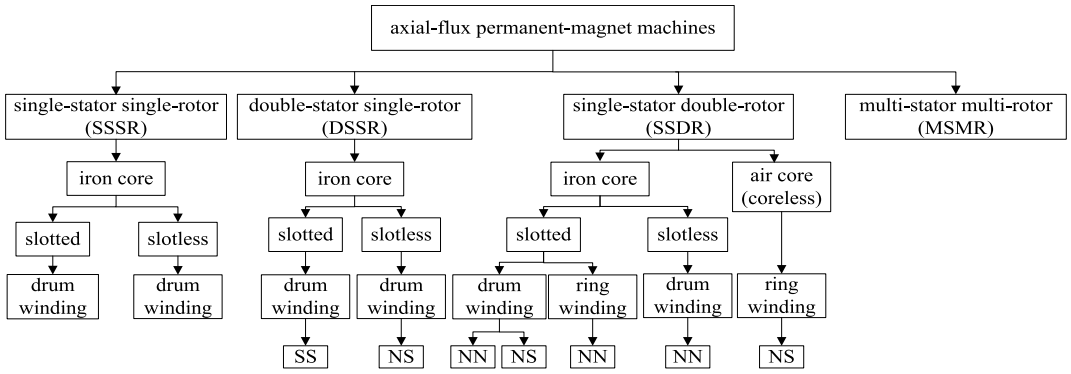

Fig. 1. Various topologies of AFPM machines.

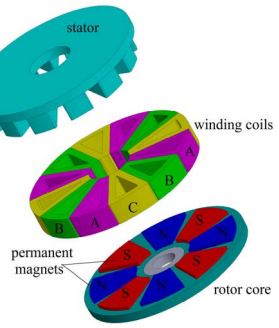

Fig. 2. 3-D view of a four-pole-pair/12-slot SSSR AFPM machine.

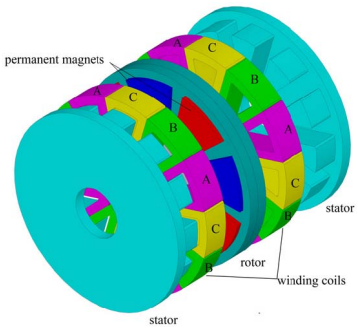

Fig. 3. 3-D view of a four-pole-pair/12-slot DSSR AFPM machine.

AFPM machine. It is a 3-D diagram of the 12 slots, four pole pairs SSSR AFPM machine with concentrated winding known as nonoverlapping windings. However, distributed winding is also applicable. The SSSR AFPM machines have applications in industrial traction, servo electromechanical drives, military, transportation industries, and gearless elevators because of its compact structure and high torque capability [6]. The major disadvantage of this machine is the imbalanced axial force between stator and rotor, which may twist the structure easily [7]. Different methods have been presented to achieve the maximum rotational torque with minimized axial force. Some of these methods are: adjusting the portions of stator winding currents projected onto the orthogonal sets of axes corresponding to the rotor positions, slotless stator, complex bearing arrangements, thicker rotor disc, and current shifting angle [8].

B. DSSR Machine

In two-stator one-rotor axial-flux interior-rotor machine, the rotor is either located between two slotted stators (SS-type) or two slotless stators (NS-type), whereas PMs are located on the surface of the rotor disc or inside the rotor disc [9]. Fig. 3 shows the 3-D diagram of the slotted double-stator single-rotor (DSSR) AFPM machine. This figure is a 3-D configuration of the motor with concentrated winding.

Fig. 4(a) and (b) shows the flux paths for the surface-mounted and interior DSSR AFPM structure, respectively. Main flux flows circumferentially along the rotor disc or axially through the rotor disc. Power density in the interior PM structure is lower than that in the surface-mounted structure because of the requirement for a thicker rotor disc.

Leakage flux of PM ends and armature reaction in interior design are higher compared with that of the surface-mounted design because PMs are surrounded by ferromagnetic material. However, the buried PM structure better protects PMs against mechanical impact, wear, and corrosion [10].

In another DSSR AFPM structure, the steel rotor disc is eliminated based on the main flux path [11]. Fig. 4(c) shows that the main flux does not travel through the rotor. In this structure, a nonmagnetic material such as aluminum is used to fill the spaces between the PMs and construct a rigid structure. This process generates high power to inertia ratio because of the lack of iron in the rotor, which makes this structure suitable for small inertia applications.

The copper loss in DSSR AFPM machines is high because of the long end windings. Whereas, slotted stator construction shows lower copper loss and consequently higher efficiency compared with the slotless structure [12]. A nonmagnetic material such epoxy resin is applied to fill the spaces of stator windings to improve the robustness and heat transfer in all slotless structures [13].

C. SSDR Machine

In single-stator double-rotor (SSDR) AFPM machines, the slotted or slotless stator is located between two rotors [14]. Fig. 5 shows an example of a typical SSDR machine. This figure is a 3-D configuration of the motor with concentrated winding (the same as Fig. 2 which is simply double sided).

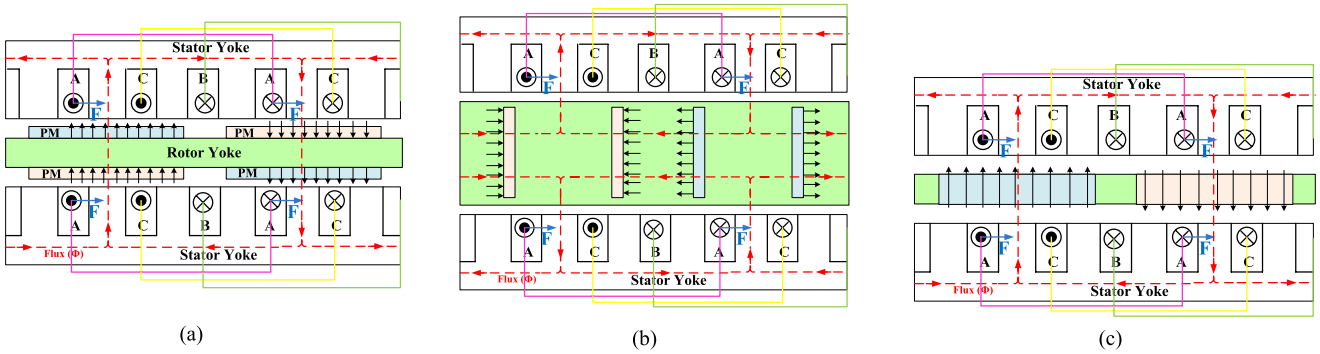

Fig. 4. Flux paths in 2-D plane for DSSR structure of the AFPM machine. (a) Surface-mounted PM structure. (b) Buried PM structure. (c) Interior PM structure without steel disc.

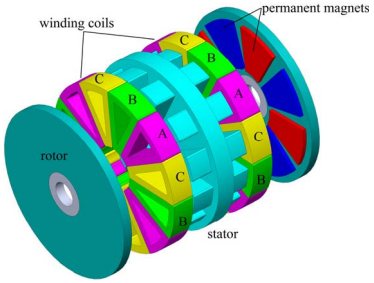

Fig. 5. 3-D view of a four-pole-pair/12-slot SSDR AFPM machine.

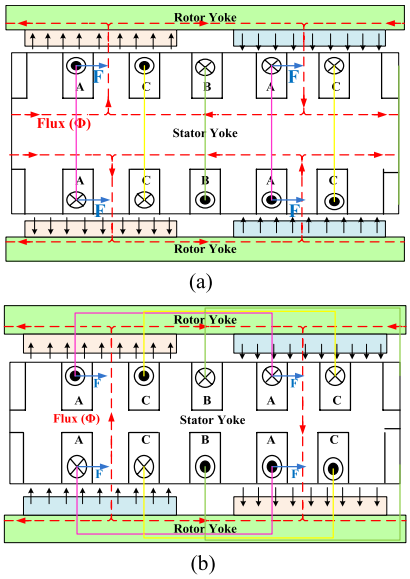

Fig. 6. Flux paths in 2-D plane for SSDR AFPM machine. (a) NN PM structure. (b) NS PM structure.

In SSDR topology, the main flux either travels axially through the stator or circumferentially in the stator yoke while the torque is generated by the radial direction windings [15]. In slotless machines, end windings are short, such that less copper loss and better heat dissipation are achieved. Leakage and mutual inductance in a slotless configuration are also lower. Therefore, slot effects such as flux ripple, cogging torque, high-frequency rotor loss, and stator teeth are eliminated [16]. Flux direction of the slotted SSDR AFPM machine with NN and NS PM arrangements are presented in Fig. 6(a) and (b), respectively.

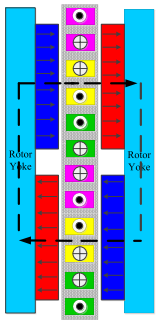

Fig. 7. Coreless NS TORUS structure of the AFPM machine.

These structures have different stator-yoke thicknesses and winding arrangements. In NN structure, the wound phase winding around the stator core (ring windings) in both the axial and radial directions is short. As a result, a thick stator yoke is necessary for the total flux entering the stator from both rotors, which enhances the iron loss and lengthens end windings. In NS structure, main flux travels axially through the stator, which makes the stator yoke unnecessary. In this case, iron loss is reduced. However, drum windings are required for NS configuration which lengthen end windings and increase the external diameter of machine to produce torque [17].

Another SSDR machine is the coreless AFPM machine (Fig. 7) [18]. In this machine, main flux travels from one rotor to another rather than passing circumferentially along the stator core. The stator and rotor include only windings and surface PMs, respectively. The efficiency could be very high with the application of strong PMs due to the absence of iron loss [19]. This structure is mainly preferred in applications that less cogging torque and torque ripple are tolerated.

D. MSMR Machine

A multistage AFPM machine can be constructed from either DSSR or SSDR configurations [20]. This machine includes the N stators and $N+1$ rotors that have the same mechanical shaft. The stator windings can be connected either in parallel or in series. The multistage configuration enhances the torque and power density without increasing the machine diameter. Among multistage AFPM and RFPM machines, AFPM ones can be more easily assembled because of their planar air-gap.

The MSMR AFPM machines may include slotted or slotless, iron core or ironless, NN or NS topologies while

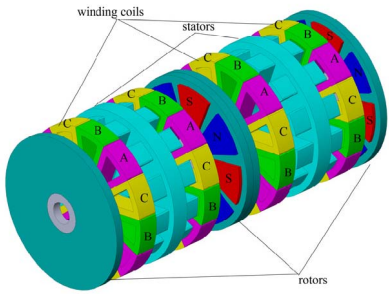

Fig. 8. 3-D view of a four-pole-pair/12-slot multistage AFPM machine ($N = 2$ stator; $N + 1 = 3$ rotors).

their flux paths are the same as their single-stage structures. The advantages and disadvantages of each construction are similar to their relevant preceding structures. The multistage AFPM machines have applications in ship propulsions, pumps, and high-speed PM generators [21]. Fig. 8 shows a 3-D diagram of a multistage AFPM machine.

III. AFPM Machine Design and Sizing Equation

A. Sizing Equation

The initial step in AFPM machine design is the selection of suitable volume of PMs, dimensions of stators, and rotors based on various constraints such as rated/maximum torque, rated/maximum speed, maximum allowable geometric dimensions, cooling method, maximum line-to-line voltage, phase current, etc. Sizing equation is proposed to determine the construction and dimensions of the AFPM motor including number of phases, stator slots, PM volume, outer and inner diameter of the stator and rotor, and air-gap length [22], [23]. If the resistance and leakage inductance of the stator are negligible, the output power of the electrical machine is calculated as

$$P_{\text{out}} = \eta \frac{m}{T} \int_0^T e(t)\, i(t) dt = \eta m K_p E_{\text{pk}} I_{\text{pk}} \tag{1}$$

where $i(t)$ is the phase current, m is the number of machine phases, $e(t)$ is the phase air-gap EMF, η is machine efficiency, K_p is the electrical power waveform factor, T is the period of one EMF cycle, and E_{pk} and I_{pk} are the peaks of phase air-gap EMF and of current, respectively [24]. K_p and E_{pk} are defined as

$$K_p = \int_0^T \frac{e(t) \cdot i(t)}{E_{\text{pk}} \cdot I_{\text{pk}}} dt \tag{2}$$

$$E_{\text{pk}} = K_e N_{\text{ph}} B_g \frac{f}{p} \left(1 - \lambda^2\right) D_o^2 \tag{3}$$

where K_e is the EMF factor incorporating winding distribution factor and per-unit portion of air-gap area total spanned by salient poles of the machine (if any), N_{ph} is the number of winding turns per phase, B_g is the flux density in air-gap, f is the converter frequency, p is the machine pole pairs, λ is the diameter ratio D_i/D_o of the AFPM machine, D_o is the diameter of outer surface of the machine, and D_i is the diameter of the inner surface of the machine. A general-purpose sizing equation for AFPM machines takes the following form [24]:

$$P_{\text{out}} = \frac{1}{1 + K_\phi} \frac{m}{m_1} \frac{\pi}{2} K_e K_i K_p K_L \eta B_g A \times \frac{f}{p} (1 - \lambda^2) \left(\frac{1 + \lambda}{2} \right) D_o^2 L_e \tag{4}$$

where m_1 is the number of phases of each stator, L_e is the effective axial length of the motor, K_ϕ is the electrical loading ratio on the rotor and stator, K_i is the current waveform factor (the ratio between the peak value and the rms value), and K_L is the aspect ratio coefficient pertinent to a specific machine structure, considering effects of loss, temperature rise, and the efficiency requirements of the design. The diameter ratio λ is the most important design parameter and has a significant effect on machine characteristics. The value of λ must be carefully chosen to optimize machine performance. Machine power density for total volume is defined as

$$p_{\text{den}} = \frac{P_{\text{out}}}{\frac{\pi}{4} D_{\text{tot}}^2 L_{\text{tot}}} \tag{5}$$

where D_{tot} and L_{tot} are the total outer diameter and total length of the machine, respectively, including the outer diameter and end winding protrusion of the stack from the radial and axial iron stacks.

B. Design Optimization

A general optimization process for an AFPM machine is possible with shape modification through the choice of geometrical parameters, deterministic methods, or soft computing methods [25]–[32]. Aydin *et al.* [25] developed optimum-sized AFPM machines for both SSDR and DSSR topologies, but only two parameters (diameter ratio and air-gap flux density) are considered as optimization variables, and the optimization was conducted through the shape modification. In all shape-modification methods, there are tradeoffs among the performance parameters, and the methods are not applicable to the multiobjective optimization problems. In some studies, the optimized value of $1/\sqrt{3} \approx 0.58$ for the ratio (λ) of inner diameter to the outer diameter was chosen to maximize the output power in AFPM machines [26].

Yang *et al.* [27] presented an optimal design of an AFPM machine using sensitivity analysis and a magnetic circuit model. The preliminary motor shapes were obtained by optimizing the cost function. Finite element analysis (FEA) was performed on the electromagnetic, thermal, and dynamical characteristics. The considered objectives include the output torque, efficiency, and torque density. Hwang *et al.* [28] presented an optimum design of a coreless SSDR AFPM machine using Taguchi method. The analysis and simulations were conducted by FEA. Taguchi's parameter design method provides a systematic approach to conduct the numerical experiments to determine near optimum settings of the design parameters. The only studied objectives include minimization of the ratio between torque ripple and average torque.

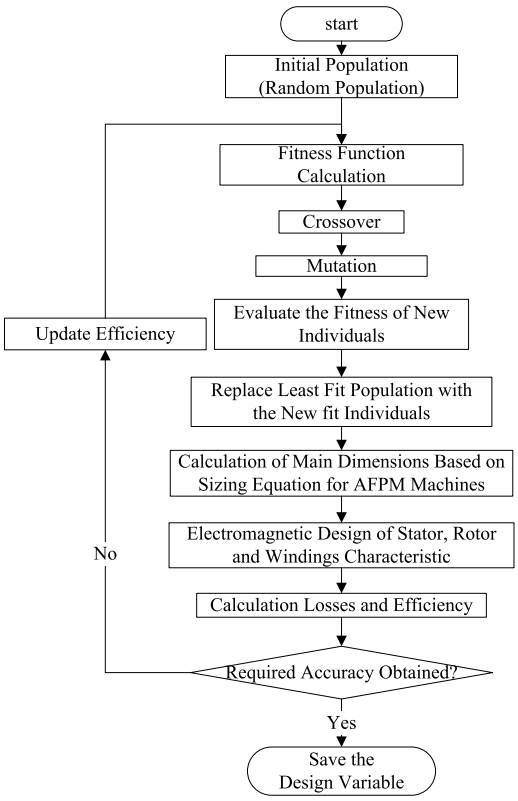

Fig. 9. Flowchart for GA-based design optimization of AFPM machine.

Soft computing methods are proposed as a solution for multiobjective optimization problems because of highly effective computer systems and novel, fast-computing algorithms. Standard optimization techniques include the random search method, Hook and Jeeves method, Powell method, and genetic algorithm (GA) [28]. The random search method requires a long time to converge and depends entirely on the starting point, whereas the Hook and Jeeves method is slower but more accurate [29]. The Powell method rapidly achieves an optimal solution but is not as robust when faced with more complex problems or if the desired global minimum is hidden among several local minimums. Rostami *et al.* [30] reported an optimized design of a variable-speed AFPM synchronous generator. 3-D FEA is conducted to simulate the GA results with the objective of minimizing the active cost while limited simulation results are presented. Mahmoudi *et al.* [31] conducted GA-based sizing equation with performance analysis via FEA to optimize a 1 kW, 3-phase, 50 Hz, four-pole AFPM synchronous motor based on the practical limitations for a typical scooter. The considered design objectives include maximum power density, cogging torque minimization, and minimum THD of the induced EMF. Fig. 9 shows the flowchart of a generalized optimization of the AFPM motor using GA.

Kahourzade *et al.* [32] presented the optimized design of a 1 kW, three-phase, 50 Hz, four-pole SSDR AFPM machine. The GA is used to optimize the dimensions of the machine to achieve the highest power density. Electromagnetic field analysis of the candidate machines from GA with various dimensions is then put through FEA to obtain various motor characteristics. With the results from GA and FEA, new candidates are introduced and then put through (finite volume analysis) FVA for thermal behavior evaluation of the designed motors. Techniques like modifying the winding configuration and skewing the permanent magnets are also investigated to attain the most sinusoidal back-EMF waveform and reduced cogging torque. The performance of the designed machine is tested in simulation using FEA software. It is found that the simulation results agree with the designed technical specifications. It is also found from FVA results that the motor temperature reaches at highest temperature to 87 °C at the rated speed and full load under steady-state condition.

IV. Analysis of AFPM Machine

A. Electromagnetic Analysis

The electromagnetic field of AFPM machine is calculated using the analytical model, quasi 3-D analytical model, method of image, 2-D finite element method (FEM), and 3-D FEM [33]–[37]. Needleless to say, 3-D FEM is more accurate as compared to the analytical method and 2-D FEM. It is capable of solving complicated problems with integral or partial differential equations. However, FEM is time consuming and requires large memory capacity. To overcome these problems, some researchers have been conducted in electromagnetic analysis of AFPM machines using analytical models, which achieve acceptable results similar to FEM.

Sung *et al.* [33] proposed the electromagnetic field analysis of an SSDR AFPM generator using improved quasi-3-D and Maxwell's equations. An analytical approach to analyze the magnetic field distribution and estimate the equivalent circuit parameters are presented that dramatically reduces the analysis time while maintaining high reliability. The designed generator has slotless stator core for cogging torque reduction and ring-wound type coils that are placed in the stator core. The flux leakage was considered because it is dominant in the inner and outer radii of this type of machine. The experimental tests verify all of the analysis results.

Lee *et al.* [34] proposed method of image using magnetic charge to analyze characteristics of the slotless AFPM motors. The method of image replaces the effects of a boundary on an applied field by simple distributions of current or charges behind the boundary line. The desired field is achieved by the sum of applied and image fields. Method of image is required for the field on each side of a boundary, but the knowledge of one group of images leads to the other, since the solutions for the two regions are connected by the boundary conditions. Mechanical stability is enhanced by the reduction of normal force affects vibration and noise. Comparison between calculated and experimental results indicates some deviations. For instance, approximately 8% error at the peak value of back-EMF due to saturation in magnetic circuits.

Chan *et al.* [35] proposed an analytical mean radius model for an ironless single-sided AFPM synchronous generator. Laplace equations are solved in the rectangular coordinate system to calculate the scalar magnetic potentials using a Fourier series method. A multicurrent-sheet model is conducted to calculate the armature reaction field, considering distributed armature conductors. To verify the accuracy of the analytical results, the magnetic field was also computed using 2-D FEM.

The analytical results give slightly higher field values, but, in general, the errors are within 3% of the computed results from FEM.

Huang *et al.* [36] presented a magnetic field analysis of an ironless AFPM machine under open-circuit condition using 3-D analytical modeling based on the magnetic scalar potential and the cylindrical coordinate. The method involves the analytical solution of the governing field equations in the region between back-irons in the cylindrical coordinate. In this region, the PMs are assumed to be axially magnetized and have constant relative recoil permeability. The analytical results were concluded to be in good agreement with those of 3-D FEA.

De la Barriere *et al.* [37] presented a 3-D analytical model of an AFPM synchronous machine based on Maxwell equations. The analytical solution of the Laplace equation gives the scalar magnetic potential in cylindrical coordinates. Fourier Bessel series have been introduced for taking into account the radial edge effects of the machine. Another original point is then use of a modulation function for considering the iron parts edge effects. The model is validated by 3-D FEM computations, for a computation time 95% lower than FEM. The electromagnetic model should be improved for taking into account the machine saliency in three dimensions, which remains as a challenging but necessary task.

B. Cogging Torque Analysis

The cogging torque is generated by the interaction between the excitation and the air-gap harmonic permeance. In PM machines, cogging torque arises from the PMs' tendency to align themselves in the minimum reluctance path given by the relative position between the rotor and stator [38]. The cogging torque causes vibration and noise as well as weakens the high-performance motion control response, particularly at low-speed and light loads. Cogging torque is calculated using stored magnetic energy in the free space [39] or the Maxwell stress tensor [40]. Among the various publications on cogging torque reduction in the AFPM machines, some recent achievements are explained in the following paragraphs [41]–[46]. Aydin *et al.* [41] minimized the cogging torque value by applying cogging torque phase angle changing. This was achieved by alternatively using two PM pole arcs and simultaneously reducing the amplitude of each portion. The test results show that the peak cogging torque is as low as 8.8% of the rated torque.

Letelier *et al.* [42] studied the effect of stator slot displacement and PM skewing in reducing cogging torque. Stator slot displacement reduces the cogging torque value close to 50%. However, the frequency of the cogging waveform doubled, and the average torque decreased. The most important influence of the skew angle is cogging variation for symmetrical and asymmetrical rotor pole positions.

González *et al.* [43] investigated the effect of the PM shape and stator side displacement on the cogging torque and electromagnetic torque. Authors used both concave and convex PM shapes to reduce the cogging torque but the reductions for both of them were found to be the same (approximately 60%). However, the concave PM generates 2% higher electromagnetic torque than that of the convex PM machine.

Brown *et al.* [44] analyzed the effect of stator manufacturing error on the cogging torque. A superposition method is applied to predict critical cogging harmonics for an AFPM synchronous motor considering the interaction between a single slot and a single lamination. The image-processing method is applied to obtain the stator geometry and the manufacturing tolerances of a single-stator slot. Experimental results validate the predicted values and the proposed image-processing technique.

Woo *et al.* [45] proposed a multimodal optimization method called climbing method. The advantage of this algorithm is that it finds all the peaks in the problem domain by calling as few functions as possible through the contour line concept coupled with Krigin. Magnet skewing and magnet pole-arc to pole-pitch ratio are considered as design variables to obtain minimum cogging torque. The proposed algorithm decreases the cogging torque value by 79.8%.

Donato *et al.* [46] investigated the influence of integral-slot and fractional-slot concentrated windings on the performances of SSDR AFPM machines. The peak cogging torque for the integral-slot concentrated windings design is approximately three times of the fractional-slot concentrated windings. Torque ripple under load conditions is higher for the integral-slot concentrated windings.

C. Thermal Analysis

The optimal design of an AFPM machine includes electrical and mechanical developments as well as thermal and fluid dynamic features. Although the electromagnetic analysis of the AFPM machines has been studied extensively, limited attention has been directed toward its thermal and aerodynamic aspects [47]. In an electrical machine, the internal temperatures must be predicted during design because of the following reasons [48]:

1) limited tolerance of continuous maximum temperatures for materials such as polymers (applied in the stator construction) and the risk of demagnetization of PMs [4];
2) dependency of efficiency on the stator temperature attributed to copper loss;
3) limitation of maximum current density and torque density in the maximum temperature;
4) excessive safety margins and, consequently, cost of inaccurate predictions.

Thermal analysis techniques include the experiment method, numerical analysis, and lumped-parameter (LP) thermal model [49]–[56]. Fig. 10 depicts aforementioned thermal analysis methods to determine temperature zones in an AFPM motor.

The experiment method is suitable for evaluating cooling strategies with high accuracy. Sugimoto *et al.* [49] developed a high-temperature superconducting (HTS) AFPM synchronous motor at liquid nitrogen temperature. In this design, the PM is applied to the iron cores, whereas HTS wires are used as the armature. The motor has eight field poles and six armature windings. The armature is placed between the two fields.

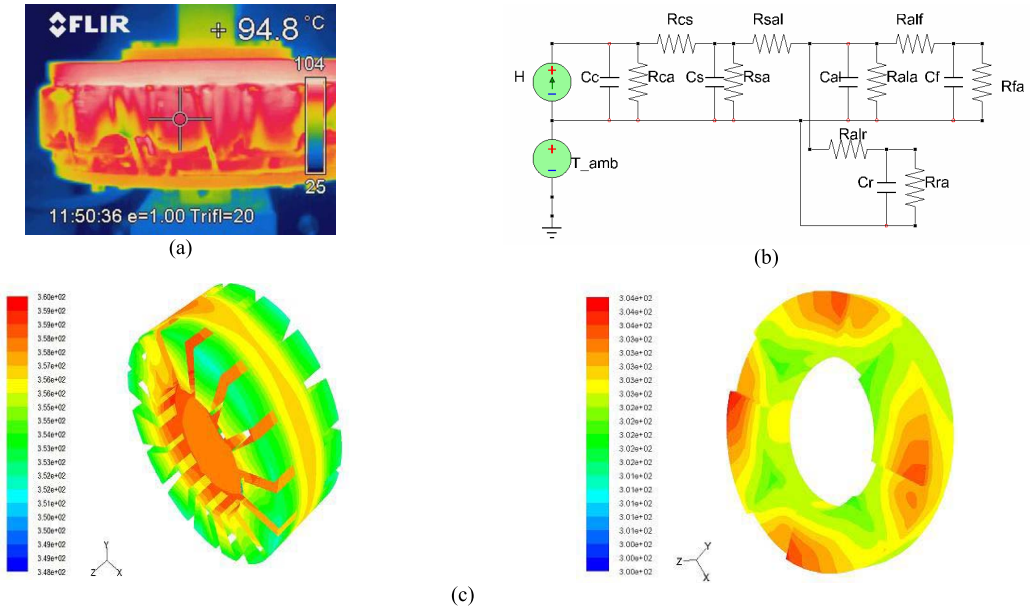

Fig. 10. Thermal analysis of an AFPM motor: experiment, lumped-parameter thermal model, and numerical analysis. (a) Infrared image of an AFPM test-machine, for determination of temperature field [55]. (b) Temperature modeling of stator surface [56]. (c) Temperature (°K) contour for both rotor and stator of the motor representing the thermal distribution [32].

The BSCCO wires, which are applied to armature windings, work at temperatures between 66 and 70 K. However, superconducting wires exhibit AC losses if they are operated at alternating magnetic fields.

The numerical methods, which are usually FEA-based or FVA-based, calculate generated losses in various regions, which act as the heat sources in the thermal analysis. Recently, the diffusion of commercial software packages that enable coupled computational fluid dynamic (CFD) and FEA have given researchers a powerful tool to perform complex simulations of 3-D heat generation, flow, and exchange in AFPM machines [50].

Marignetti *et al.* [51] studied the thermal characteristics of an AFPM synchronous machine with a soft magnetic compound (SMC) core using 3-D-FEA. The thermal source is achieved from a dc current flow model coupled to the magneto static solver, thermal, and fluid-dynamical model. The disadvantage of the method is that the results are very sensitive to possible inaccuracy, thus affecting boundary condition placement. In addition, the rotor core of the prototype model is significantly hotter than the simulation results. The operational temperature under the 403 °K is required by the epoxy.

Howey *et al.* [52], studied stator convective heat transfer by using CFD modeling. A thin-film electrical heating method provides radially resolved steady-state heat-transfer data from an experimental rotor-stator system designed as a geometric model of a through-flow ventilated AFPM machine. Experimental results confirm that the predicted stator heat transfer is almost insensitive to the turbulence model used in the CFD simulations.

The LP model depicts thermal problems through a thermal network similar to an electrical circuit. Lim *et al.* [53] proposed an LP model for a six-pole slotless SSDR AFPM generator based on a simplified axisymmetric model. The components of the generator and the internal air-flow domain are split into a system of connected and interacting control volumes. To determine the thermal condition, energy and mass conservation equations are solved for each volume while considering the heat transfer attributed to conduction and convection. The accuracy of results is verified by comparing with CFD results.

Rostami *et al.* [54] presented an LP model for solving the steady-state thermal problem of a DSSR AFPM generator. The model derives the temperatures in the stator windings and PMs. The LP model is derived from purely dimensional data and the material properties of the machine components. Iterative coupled electromagnetic and thermal designs are applied because of the material temperature-dependent thermal properties. Experimental results of the designed machine verify the accuracy of the thermal resistance network in terms of predicting the nodal temperatures.

D. Mechanical Analysis and Manufacturing

Mechanical analysis has an important function in the design of an AFPM machine considering the effect of machine dimensions on its transient and steady-state performances, such as the dependency of centrifugal force on the PM lengths or axial attractive forces on the air-gap length [57]–[63]. In this section, articles on the structure and mechanical analysis of AFPM machines are reviewed.

Liu *et al.* [57] proposed an algorithm for linear torque control and axial force reduction of an AFPM motor applied in an electric vehicle by determining a partial derivative of the co-energy of the machine with respect to the axial direction. The axial force is a nonlinear function of the stator MMF,

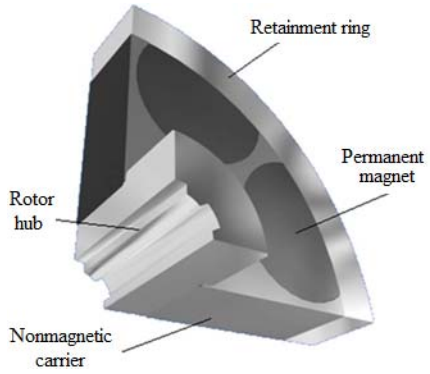

Fig. 11. Sectional view of the rotor of the high-speed modular air-cored AFPM generator.

PM flux, and demagnetizing d-axis current component. The proposed single-sided AFPM motor shows full operational controllability using current shifting angle method. Optimal operational performance is achieved using a current shifting angle of $(-30°)$ degrees.

Vansompel *et al.* [58] presented the efficiency optimization of an AFPM synchronous generator with concentrated pole winding. A 3.6-kW 2000-r/min eight-pole pair AFPM generator for combined heat and power applications is prototyped and tested. To reduce losses, concentrated pole windings, and segmented PMs, a thin grain-oriented material for stator teeth are applied in the design. The FEM and the analytical methods are applied to study the effect of mass on the optimal values of parameters and on efficiency. The flat course near the point of maximum efficiency in the mass-efficiency curve shows that a drastic reduction in mass results in slight efficiency reduction, which has an essential impact on the cost and portability of the machine.

Fei *et al.* [59] presented a mechanical design of a high-speed modular air-cored AFPM generator with focus on electromagnetic optimization. Fig. 11 shows the designed rotor, which includes the PMs, retainment ring, and back iron. A rigid, high-strength rotor hub connects the PM rotor disc and shaft. The rotor hub is shrunk to fit at the bore of the magnet rotor disc to prevent slippage of the magnet rotor at high operating speed and is coupled with other rotor hubs on the same shaft through mechanical splines. It is reported that during the acceleration of the rotor to the maximum speed, slight vibrations of the rotor were observed at 22 300 and 39 000 r/min, which is related to the different natural frequencies caused by the combinations of different rotor parts. Apart from these two speeds, the rotor runs smoothly without experiencing any noticeable vibration.

Di Gerlando *et al.* [60] designed and tested a 50 kW, 70 r/min, 19-pole pair, multistage AFPM direct-drive wind generator with concentrated windings. The paper focused on the sizing relations and electrical parameters. The machine structure implies some peculiar features: the absence of stator yokes, compactness, low rotor inertia, and low synchronous inductance. Eddy current loss is decreased by using segmented PMs because of the slotting and distributed mmf in the air gap. A strategy to reduce the free design parameters, to perform a simple parametric analysis, and to achieve an optimized design is proposed. However, extra teeth core losses happened due to the manufacturing process.

Lee *et al.* [61] compared the electromagnetic and mechanical performance of slotless AFPM machines with spiral and laminated stator. The laminated stator is found to be stiffer and simpler for manufacturing compared with those of the spiral stator. However, the laminated stator facilitates higher temperature at the magnetic core because of the increasing eddy current. The spiral stator demands higher phase current at low speed because of the increasing magnetic air-gap flux density under the same stator volume and generates more noise because of the lower stiffness of the stator.

De Donato *et al.* [62], [63] analyzed the effect of magnetic SMC wedges on the load performance of AFPM machines. A reduction in reluctance of the slot leakage path using SMC wedges enhances slot leakage inductance and shifts no-load loss significantly from the PMs to the stator. It facilitates the extraction of generated heat and reducing the danger of magnet demagnetization attributed to high temperature.

V. Field Control of AFPM Machines

The absence of excitation windings and brush contact reduce the operational cost and increase the efficiency and reliability of AFPM machines. However, the fixed flux imposed by the PMs is crucial for variable speed applications. The linear variation of the induced back-EMF voltage makes the operation dangerous at high speed. In fact, the winding insulation and inverter power semiconductor can be degraded when operated at high voltage. To avoid this unsafe operation, air-gap flux must be controlled to keep the terminal voltage at rated value. Flux weakening in brushless AFPM machines either is applied by mechanical means [64]–[66] or by control strategies [67]–[71]. Some key publications on the field weakening of AFPM motors are reviewed in the following paragraphs.

Del Ferraro *et al.* [64] proposed the mechanical flux weakening of AFPM machines by displacing two rotor discs to achieve a reduction in the stator linked flux. Desired regulation is achieved by two different mechanical solutions: mechanical speed-dependent device and mechanical torque-dependent device. The first device is a constant voltage source where the second one is a constant current source. Although their work introduces an innovative concept of mechanical flux weakening for AFPM power regulation in a wide speed range, but applied devices do not modify starting behavior, high torque density, and overload capability of the machine.

In [65], the authors proposed dual rotor shifting method for field weakening of an AFPM machine. The stator winding is split into two separate and adjacent Litz-wire windings, each one encapsulated in epoxy resin and both connected in series; the two windings are encased in a fixed frame and separated by low-friction Teflon rings. Flux-weakening is achieved by rotating the windings with respect to each other by means of a purposely designed actuator. The experimental results show proper operation of the system up to 5000 r/min and constant power speed regions ratio (CPSR) equal to 8.3 : 1.

Zhao *et al.* [66] proposed the adoption of radially sliding PMs for the field weakening and speed control of a novel AFPM machine suitable for electric vehicles (EVs). The field-weakening method with radially sliding PMs is compared and combined with traditional electrical method. The results indicate that the field control capability is improved drastically and the maximum speed (up to six times the nominal speed) with constant power is achieved.

Field weakening based on the control of the d-axis component of the armature reaction flux had been proposed. Lopez *et al.* [67] experimentally tested the field capability of a 5-kVA eight-pole AFPM machine by modifying the main magnetic circuit that reduces the value of stator ampere-turn required to control the air-gap flux. The soft iron section of the rotor pole decreases reluctance. Thus, a low d-axis stator current is required to demagnetize the machine with low magnetic and thermal stress for the magnet. However, the presented results are mostly discussed current, voltage and its harmonic spectrum instead of field control capability.

Kwon *et al.* [68] proposed field weakening of a surface-mounted AFPM synchronous machine by using slotted stator with fractional slot winding and cores enclosing end windings. In addition, a flux weakening controller is designed to use the full capability of the machine. The controller utilizes the voltage difference between the current regulator and the output voltage, limited by a voltage source inverter. The results indicates that by using this method the output torque in the field weakening region is higher than that of voltage-magnitude feedback.

Aydin *et al.* [69] presented a field-controlled AFPM machine utilizing a dc field coil located on the stator. This field winding is used to magnetize the iron poles of the rotor. Depending on the magnitude and direction of the excitation, the net air-gap flux over a pole section increases or decreases. Subsequently, the air-gap flux densities resulting from different dc excitations acting on the machine stator winding vary, and the induced EMF decreases or increases. Thus, the operating rang of AFPM machine can be extended.

VI. Line-Start Axial-Flux Permanent-Magnet Synchronous Machine

Line-start permanent-magnet (LSPM) motors can be a substitute for induction motors in constant-speed applications such as fans, pumps, and compressors because of their higher efficiency, power factor, power density, and smaller size. These motors, however, have poor starting torque and poor synchronization. The starting and synchronization of LSPM motors have been the subject of numerous studies. However, the focus has been on line-start radial-flux permanent-magnet (LSRFPM) motors [72]–[75], whereas few publications on line-start axial-flux permanent-magnet (LSAFPM) motors have been available until recently [76]–[78].

Mahmoudi *et al.* [76] proposed the LSAFPM motor for the first time. A spaced and raised ring is added to the inner radii of the rotor disc for auto-starting. This ring partially covers the inner yoke of the stator. The interaction between the induced eddy-currents in the solid rotor rings and the rotating field in the air-gap between the rings and the inner end winding produces electromagnetic torque. In an AFPM motor, radial windings usually produce torque, whereas end windings are redundant, but in this work, inner end windings also produce torque. Fig. 12 shows the exploded diagram of the designed LSAFPM motor. The paper verified the successful design of a 1/3-hP, four-pole, auto-start, slotless AFPM motor with good synchronization at rated speed.

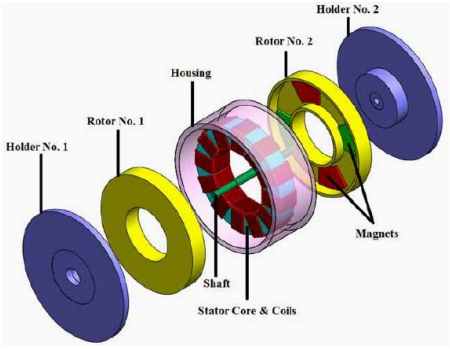

Fig. 12. Exploded diagram of the designed motor [76].

Fig. 13. Snapshot of the prototype LSAFPM motor [78].

Mahmoudi *et al.* [77] presented two design and analysis cases of an LSAFPM motor: with solid rotor and with composite rotor. Two concentric unilevel spaced raised rings are added to the inner and outer radii of the rotors to enable auto-start capability. The composite rotor is coated by a thin (0.05 mm) layer of copper. Results of the 3-D transient FEA show the composite rotor significantly improves both starting torque and synchronization capability over the solid rotor. The thin layer of copper on the rotor-ring surface increases the conductivity of the material and caused more current to circulate on the rotor-ring surface during startup. The composite rotor outperforms the solid rotor through faster start-up and shorter settling time.

In [78], the same authors presented the prototyping of the solid LSAFPM motor. It is found that the prototype motor maintains high starting torque and good synchronization. The motor is suitable for widely use in high-performance applications, where low noise and smooth torque are imperative requirements, especially where high speed is requisite. Fig. 13 shows a snapshot of the prototype LSAFPM motor. Further researches regarding line start capability of the AFPM is requisite.

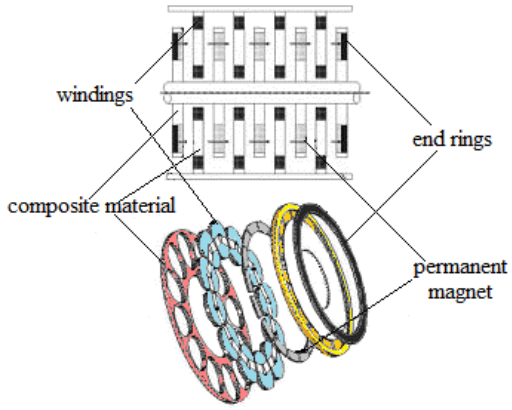

Fig. 14. Basic components of the designed axial-flux motor.

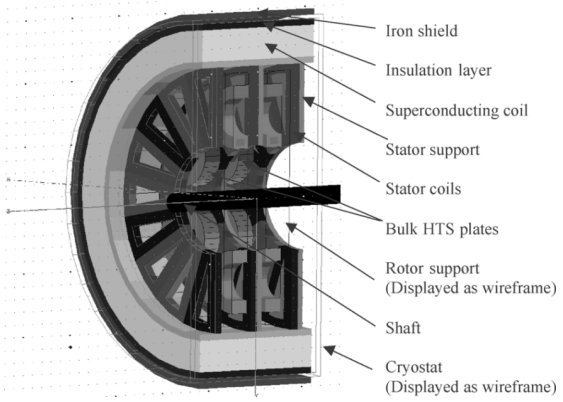

Fig. 15. High temperature superconducting axial-flux motor for aircraft propulsion design [81].

VII. Materials

The demand for electrical machines with low weight, reduced loss, and increased power density has resulted in comprehensive studies on the application of new materials in the structure of AFPM machines. Application of amorphous magnetic materials (AMM), soft magnetic composites (SMC), grain oriented steel, charged polymers, superconductors, redundant material, and plastic in construction of AFPM machines have been reviewed in recent articles [79]–[86].

Eastham *et al.* [79] developed an AFPM machine utilizing four plastic discs as the rotor disc, two internal discs to support PMs, and two external discs to support PMs, in addition to one iron ring for flux path closure. The stator consists of three larger diameter discs containing coils. Fig. 14 shows the half-section scheme and the design construction. The composite materials in the construction are nonconductive. Thus, the loss in the two iron rings is attributed only to small space harmonic fluxes and hence, the efficiency of the machine is improved.

Holmes *et al.* [80] constructed a DSSR AFPM micropower generator from a polymer rotor with embedded PMs sandwiched between two silicon stators with electroplated planar coils. The effect of design elements such as the number of layers of stator coils, air-gap length, and application of soft magnetic pole pieces on the stators have been investigated. It was concluded that higher output powers could be achieved by reducing the rotor-stator gap, enhancing the coil fill-factor increasing the number of poles, or increasing the number of coil layers on each stator.

Masson *et al.* [81] proposed a high-temperature superconducting (HTC) axial-flux motor for aircraft propulsion. Experimental data shows that utilizing superconducting yttrium barium copper oxide (YBCO) pellets instead of conventional PMs increases the capacity of magnetic flux up to 17 T at 29 °K with approximately 18 Nm/kg torque density, and 99% efficiency. Fig. 15 shows the motor conceptual design and its components.

Sharkh *et al.* [82] proposed a double-gap AFPM dc motor with double-layer armature wave winding constructed of copper strips. The authors compared the performance of two AFPM machines using powder iron and laminated steel materials as armature teeth. The FEA and experimental results prove that the steel laminated motor has better performance than the powder iron motor because of the higher permeability and higher saturation flux density of powder iron. The powder machine has lower back EMF, lower torque capability, lower air-gap flux density, and lower efficiency compared with that of laminated stator.

Kowal *et al.* [83] studied the performance and iron loss of an AFPM synchronous machine using nonoriented (NO) steel and iron-loss-enhancing grain-oriented (GO) material via FEM. The magnetic energy is calculated using several measured quasi-static-loops on an Epstein frame in seven directions starting from the rolling direction to the transverse direction. Loss is calculated based on the principles of loss separation and dynamic loop measurements for each of the seven directions, assuming unidirectional fields. The machine with GO material has approximately seven times less iron loss at the same speed and 10% higher torque under the same current. However, the back-EMF waveforms at no-load are almost the same for both materials.

Marignetti *et al.* [84] compared two AFPM synchronous machines with the same stator made of ATOMET-EM1 SMC with solid-steel rotor core and ATOMET-EM1 SMC rotor core. The SMC rotor presents magnetic saliency attributed to saturation. The AFPM synchronous machine with SMC rotor achieves higher efficiency and power density. The no-load loss declines by 19%, and the efficiency increases by 12%. Moreover, the AFPM synchronous machine with SMC rotor has double the thermal current limitation.

Wang *et al.* [85] designed and tested an AFPM motor by using amorphous magnetic materials as cut cores in the stator and ferrite magnets in the rotor. The combination of AMM cut cores and ferrite magnets increases the efficiency up to 90%. It is found that cut cores conserve motor space, and magnets with left–right asymmetric skewed shapes provide the optimal option to balance the induced voltage and cogging torque.

VIII. AFPM Machine Application

The AFPM machine usage has expanded from domestic to industrial applications. Some examples of AFPM machine applications are washing machines, aircraft propulsions, portable gensets, starter/alternators, wind generators, and EVs [87]–[105]. In this section, AFPM machine applications as

wind generators and EVs presented in the recent articles are reviewed because of the popularity of AFPM machines for these applications.

The AFPM synchronous generator is considered to be a suitable energy converter for direct-coupled wind turbine applications [87], [88]. Coreless AFPM generators are proposed for various power generation applications, particularly in direct-drives over a wide operational speed range. Low cogging torque and high efficiency caused by the elimination of stator teeth and back-iron yoke are the advantages of a coreless design [89].

Brisset *et al.* [90] determined the best configuration of 5-MW nine-phase concentrated-winding direct-drive wind generator. Analytical sizing model and multiobjective optimization are applied to minimize the total active mass and to maximize the power factor considering the technological constraints and temperatures. Pareto front method is used to select the best configuration and design parameter values among six different configurations.

Lee *et al.* [91] proposed the design optimization of an AFPM generator for battery charging applications. The design objects include size, weight, and efficiency. Size optimization is achieved by applying an SMC core instead of a silicon steel core. Although some differences exist between the simulation and experimental results because of the air-gap prototyping error, the authors claim that the proposed generator is capable of charging a 50-Wh battery within the speed boundary which is based on the design specifications.

The concept of applying AFPM motors in EVs was first proposed in the 1990s. Over the past 20 years, several studies have been conducted on the design of AFPM machines to optimize the performance of EVs. Oh *et al.* [92] simulate and test the capability of an AFPM motor for hybrid EVs by using a vehicle simulator. The efficiency map of the motor is developed for various operating conditions. The performance of the motor for various drive cycles and optimal air-gap values is determined based on the hardware in loop concept. The motor speed follows the speed commands under variable gap conditions. The advantages of the design include extended operating speed range and high efficiency.

Rahman *et al.* [93] presented a direct-drive SSDR AFPM motor for fuel cell EV and HEV propulsion application. Adding magnetic wedges in the stator slots increases the power range by more than two times. This process also decreases core loss and increases efficiency. Power loss is minimized by the application of high thermal conductivity epoxy joining machine stator and liquid-cooled aluminum casing. The mass of the machine, as well as cogging torque and torque ripple, is minimized.

Yang *et al.* [94] proposed the optimal design and control of an SSDR AFPM motor mounted inside the wheel without mechanical transmission and differential gears for electric passenger cars. The FEA results indicate that the design has the capability to drive a 600-kg passenger car with acceleration from 0 to 40 km/h in 5 s on a 15° incline. Critical design parameters including maximum torque, efficiency, rated speed, minimum weight, materials, and power source are determined using sensitivity analyses.

Nguyen *et al.* [95] proposed an AFPM machine designed for a flywheel energy storage system with the objective of achieving high efficiency, zero fundamental frequency rotor loss, low cogging torque, and improved back-EMF waveforms. The design includes two sets of three-phase stator windings and requires only one power converter to supply power for the control of both axial force and electromagnetic torque. The optimal PM skew angle to achieve the minimum cogging torque, considering minimum effect on the static axial force, is presented.

In addition to the mentioned applications, AFPM machines are becoming popular in other industries such as, ship propulsion [96], direct drive elevator [97], hard disc [98], micropower generator [99], induction heating genes [100], slim vortex pump [101], flywheel energy storage system [102], automobile alternator [103], [104], and microenergy storage system [105].

IX. Comparison

Performance comparison among AFPM machines, RFPM machines, and transverse flux PM (TFPM) machines have been studied extensively [106]–[110]. This section reviews the publication conducted on the performance comparison of different PM machines.

In [106], authors compared the performance of AFPM machine with the RFPM machine considering following criteria: required copper, steel, and magnet weights, copper and iron loss, moment of inertia, torque per unit moment of inertia, power per unit active weight, and power per unit active volume. The presented results are based on the performance of the RFPM machine and four AFPM configurations including the slotted and slotless SSSR AFPM and the slotted and slotless DSSR AFPM topologies. For five various output power levels, it is concluded that AFPM machines are more promising in terms of volume, power density, required iron, active weight, torque, and rotor moment of inertia. The required PM material for the slotless AFPM machines is more than the RFPM machine. However, the slotted AFPM machines requires less. The copper loss in the slotless DSSR AFPM machines is higher than that of the slotted RFPM field machine.

Cavagnino *et al.* [107] compared the DSSR AFPM motor performance with RFPM machine in terms of provided electromagnetic torque and torque density, when the overall motor volume, losses per surface, and the air-gap flux density are kept constant. The pole numbers influence and the end-windings encumbrances are also take into account. The proposed procedure is based on simple thermal considerations. The results indicate that AFPM configuration has better performance in terms of electromagnetic torque and torque density if the number of poles is high (more than 10) and the axial length is short.

Chen *et al.* [108] performed the comparison among the RFPM, multistage AFPM, and three-phase TFPM machines under small current density, small electrical loading, high temperature, constant speed, and without an external cooling system condition. It was concluded that owing to the limited outer diameter, the multistage AFPM topology is not suitable

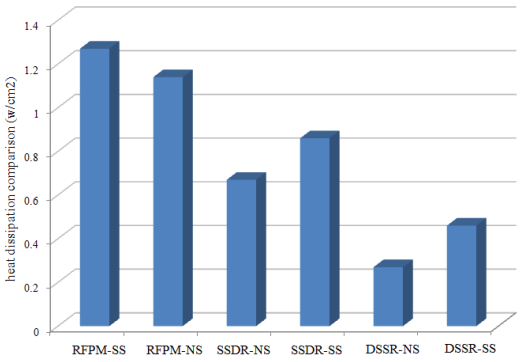

Fig. 16. Heat dissipation comparison of 200 HP, six-pole 1200 r/min radial and axial-flux surface-mounted permanent magnet machines [110].

as it has low torque density and low efficiency; the TFPM topology has high torque density but a low power factor; the RFPM machine has a simple construction, a high torque density and the best power factor; therefore, it is declared the most suitable within these design constraints.

Pippuri *et al.* [109] compared the torque density RFPM, AFPM, and TFPM machines of a 10-kW 200-r/min example machine. The achieved results of the Pareto optimal fronts method shows that the best RFPM motor designs in terms of efficiency and compactness have a pole pair number from 8 to 10. The AFPM topology was found to perform the best with pole pair numbers 10–12. The lowest pole pair numbers were found to be the least feasible when a compact yet energy efficient solution is sought after.

In Qu *et al.* [110] compared the performance of 200 HP, six-pole 1200-r/min RFPM and Double-sided AFPM machines considering different PM configurations using sizing equations. The results indicate that SSDR machines have higher power density and efficiency while SSDR-NS machine has the highest power/torque density ratio and efficiency. The DSSR-type machines are better than the others in terms of weight and utilization where DSSR-SS configuration has the lowest weight and highest utilization factor. The heat dissipation comparison results presented in Fig. 16 indicates DSSR-NS and RFPM-SS configurations have the best and worst dissipation capability, respectively.

X. Conclusion

A comprehensive review on the recent advances on AFPM machines has been presented in this paper. The AFPM machine topologies, design, performance analysis, field control, material selection, application, and performance in comparison with other PM machines have been considered. The design and analysis of the line-start AFPM motors have been discussed. The performance analyses including electromagnetic, cogging torque, thermal, and mechanical and manufacturing analysis have been reviewed. The application of AFPM generators in wind energy systems and AFPM motors in electric vehicles are totemic of this technology for contribution in energy saving and combating environment pollution. This paper presented the works of various eminent authors in the related publications with the aim of providing a useful guideline for researches and practicing engineers on the latest development of AFPM machines.

References

[1] Y. J. Cao, Y. K. Huang, and J. Long, "Research on axial magnetic force and rotor mechanical stress of an air-cored axial-flux permanent magnet machine based on 3D FEM," *Appl. Mech. Mater.*, vol. 105, pp. 160–163, Sep. 2012.

[2] A. Mahmoudi, S. Kahourzade, N. A. Rahim, W. P. Hew, and M. N. Uddin, "Design and prototyping of an optimised axial-flux permanent-magnet synchronous machine," *IET Electr. Power Appl.*, vol. 7, no. 5, pp. 338–349, 2013.

[3] T. Cook, "Improvement in electro-magnetic machines," U.S. Patent 1 735, Aug. 25, 1840.

[4] J. F. Gieras, R.-J. Wang, and M. J. Kamper, *Axial Flux Permanent Magnet Brushless Machines*. New York, NY, USA: Springer-Verlag, 2008.

[5] S. M. Mirimani, A. Vahedi, and F. Marignetti, "Effect of inclined static eccentricity fault in single stator-single rotor axial flux permanent magnet machines," *IEEE Trans. Magn.*, vol. 48, no. 1, pp. 143–149, Jan. 2012.

[6] H. Hakala, "Integration of motor and hoisting machine changes the elevator business," in *Proc. Int. Conf. Electr. Mach.*, 2000, pp. 1242–1245.

[7] C. Chan, "Axial-field electrical machines-design and applications," *IEEE Trans. Energy Convers.*, vol. 2, no. 2, pp. 294–300, Jun. 1987.

[8] C. T. Liu, T. S. Chiang, J. F. D. Zamora, and S. C. Lin, "Field-oriented control evaluations of a single-sided permanent magnet axial-flux motor for an electric vehicle," *IEEE Trans. Magn.*, vol. 39, no. 5, pp. 3280–3282, Sep. 2003.

[9] A. Parviainen, M. Niemela, and J. Pyrhonen, "Modeling of axial flux permanent-magnet machines," *IEEE Trans. Ind. Appl.*, vol. 40, no. 5, pp. 1333–1340, Oct. 2004.

[10] M. Aydin, H. Surong, and T. A. Lipo, "Torque quality and comparison of internal and external rotor axial flux surface-magnet disc machines," *IEEE Trans. Ind. Electron.*, vol. 53, no. 3, pp. 822–830, Jun. 2006.

[11] M. Aydin, S. Huang, and T. A. Lipo, "Axial flux permanent magnet disc machines: A review," in *Proc. Int. SPEEDAM*, Jun. 2004, pp. 61–71.

[12] A. Cavagnino, M. Lazzari, F. Profumo, and A. Tenconi, "Axial flux interior PM synchronous motor: Parameters identification and steady-state performance measurements," *IEEE Trans. Ind. Appl.*, vol. 36, no. 6, pp. 1581–1588, Dec. 2000.

[13] F. Caricchi, F. Crescimbini, O. Honorati, G. L. Bianco, and E. Santini, "Performance of coreless-winding axial-flux permanent-magnet generator with power output at 400 Hz, 3000 r/min," *IEEE Trans. Ind. Appl.*, vol. 34, no. 6, pp. 1263–1269, Dec. 1998.

[14] F. Profumo, Z. Zheng, and A. Tenconi, "Axial flux machines drives: A new viable solution for electric cars," *IEEE Trans. Ind. Electron.*, vol. 44, no. 1, pp. 39–45, Feb. 1997.

[15] S. Huang, M. Aydin, and T. A. Lipo, "TORUS concept machines: Pre-prototyping design assessment for two major topologies," in *Proc. IEEE Ind. Appl. Conf. Rec. 36th IAS Annu. Meeting*, Oct. 2001, pp. 1619–1625.

[16] F. Caricchi, F. G. Capponi, F. Crescimbini, and L. Solero, "Experimental study on reducing cogging torque and no-load power loss in axial-flux permanent-magnet machines with slotted winding," *IEEE Trans. Ind. Appl.*, vol. 40, no. 4, pp. 1066–1075, Aug. 2004.

[17] F. Locment, E. Semail, and F. Piriou, "Design and study of a multiphase axial-flux machine," *IEEE Trans. Magn.*, vol. 42, no. 4, pp. 1427–1430, Apr. 2006.

[18] M. J. Kamper, W. R. Jie, and F. G. Rossouw, "Analysis and performance of axial flux permanent-magnet machine with air-cored nonoverlapping concentrated stator windings," *IEEE Trans. Ind. Appl.*, vol. 44, no. 5, pp. 1495–1504, Oct. 2008.

[19] N. Lombard and M. Kamper, "Analysis and performance of an ironless stator axial flux PM machine," *IEEE Trans. Energy Convers.*, vol. 14, no. 4, pp. 1051–1056, Dec. 1999.

[20] F. Caricchi, F. Crescimbini, F. Mezzetti, and E. Santini, "Multistage axial-flux PM machine for wheel direct drive," *IEEE Trans. Ind. Appl.*, vol. 32, no. 4, pp. 882–888, Aug. 1996.

[21] F. Caricchi, F. Crescimbini, and E. Santini, "Basic principle and design criteria of axial-flux PM machines having counterrotating rotors," *IEEE Trans. Ind. Appl.*, vol. 31, no. 5, pp. 1062–1068, Oct. 1995.

[22] A. Chen, R. Nilssen, and A. Nysveen, "Performance comparisons among radial-flux, multistage axial-flux, and three-phase transverse-flux PM machines for downhole applications," *IEEE Trans. Ind. Appl.*, vol. 46, no. 2, pp. 779–789, Apr. 2010.

[23] O. Kalender, Y. Ege, and S. Nazlibilek, "Design and determination of stator geometry for axial flux permanent magnet free rod rotor synchronous motor," *Measurement*, vol. 44, no. 9, pp. 1753–1760, 2011.

[24] S. Huang, J. L. F. Leonardi, and T. A. Lipo, "A comparison of power density for axial flux machines based on general purpose sizing equations," *IEEE Trans. Energy Convers.*, vol. 14, no. 2, pp. 185–192, Jun. 1999.

[25] M. Aydin, S. Hum, and T. A. Lipo, "Design and 3D electromagnetic field analysis of non-slotted and slotted TORUS type axial flux surface mounted permanent magnet disc machines," in *Proc. IEEE IEMDC*, Jun. 2001, pp. 645–651.

[26] T. Chan and L. Lai, "An axial-flux permanent-magnet synchronous generator for a direct-coupled wind-turbine system," *IEEE Trans. Energy Convers.*, vol. 22, no. 1, pp. 86–94, Mar. 2007.

[27] Y. P. Yang, Y. P. Luh, C. H. Cheung, J. P. Wang, and S. W. Wu, "Design and control of axial-flux brushless DC wheel motors for electric vehicles-part I: Multi objective optimal design and analysis," *IEEE Trans. Magn.*, vol. 40, no. 4, pp. 1873–1882, Jul. 2004.

[28] C. C. Hwang, P. L. Li, F. C. Chuang, C. T. Liu, and K. H. Huang, "Optimization for reduction of torque ripple in an axial flux permanent magnet machine," *IEEE Trans. Magn.*, vol. 45, no. 3, pp. 1760–1763, Mar. 2009.

[29] S. Rao, *Optimization Theory and Applications*. Hoboken, NJ, USA: Wiley, 1984.

[30] N. Rostami, M. R. Feyzi, J. Pyrhönen, A. Parviainen, and V. Behjat, "Genetic algorithm approach for improved design of a variable speed axial-flux permanent-magnet synchronous generator," *IEEE Trans. Magn.*, vol. 48, no. 12, pp. 4860–4865, Dec. 2012.

[31] A. Mahmoudi, S. Kahourzade, N. A. Rahim, and W. P. Hew, "Design, analysis, and prototyping of an axial-flux permanent-magnet motor based on genetic algorithm and finite element analysis," *IEEE Trans. Magn.*, vol. 49, no. 4, pp. 1479–1492, Apr. 2013.

[32] S. Kahourzade, A. Gandomkar, A. Mahmoudi, N. A. Rahim, W. P. Hew, and M. N. Uddin, "Design optimization and analysis of AFPM synchronous machine incorporating power density, thermal analysis, and back-EMF THD," *Progr. Electromag. Res.*, vol. 136, pp. 327–367, Jan. 2013.

[33] S. Y. Sung, J. H. Jeong, Y. S. Park, J. Y. Choi, and S. M. Jang, "Improved analytical modeling of axial flux machine with a double-sided permanent magnet rotor and slotless stator based on an analytical method," *IEEE Trans. Magn.*, vol. 48, no. 11, pp. 2945–2948, Nov. 2012.

[34] S. H. Lee *et al.*, "Characteristic analysis of the slotless axial-flux type brushless DC motors using image method," *IEEE Trans. Magn.*, vol. 42, no. 4, pp. 1327–1330, Apr. 2006.

[35] T. F. Chan, L. L. Lai, and S. Xie, "Field computation for an axial flux permanent-magnet synchronous generator," *IEEE Trans. Energy Convers.*, vol. 24, no. 1, pp. 1–11, Mar. 2009.

[36] Y. Huang, B. Ge, J. Dong, H. Lin, J. Zhu, and Y. Gu, "3-D analytical modeling of no-load magnetic field of ironless axial flux permanent magnet machine," *IEEE Trans. Magn.*, vol. 48, no. 11, pp. 2929–2932, Nov. 2012.

[37] O. de la Barrière, S. Hlioui, H. B. Ahmed, M. Gabsi, and M. LoBue, "3-D formal resolution of Maxwell equations for the computation of the no-load flux in an axial flux permanent-magnet synchronous machine," *IEEE Trans. Magn.*, vol. 48, no. 1, pp. 128–136, Jan. 2012.

[38] Z. Zhu and D. Howe, "Influence of design parameters on cogging torque in permanent magnet machines," *IEEE Trans. Energy Convers.*, vol. 15, no. 4, pp. 407–412, Dec. 2000.

[39] G. Barakat, T. E. Meslouhi, and B. Dakyo, "Analysis of the cogging torque behavior of a two-phase axial flux permanent magnet synchronous machine," *IEEE Trans. Magn.*, vol. 37, no. 4, pp. 2803–2805, Jul. 2001.

[40] H. Tiegna, A. Bellara, Y. Amara, and G. Barakat, "Analytical modeling of the open-circuit magnetic field in axial flux permanent-magnet machines with semi-closed slots," *IEEE Trans. Magn.*, vol. 48, no. 3, pp. 1212–1226, Mar. 2012.

[41] M. Aydin, Q. Ronghai, and T. A. Lipo, "Cogging torque minimization technique for multiple-rotor, axial-flux, surface-mounted-PM motors: Alternating magnet pole-arcs in facing rotors," in *Proc. 38th IAS Annu. Meeting Conf. Rec. Ind. Appl. Conf.*, Oct. 2003, pp. 555–561.

[42] A. B. Letelier, D. A. Gonzalez, J. A. Tapia, R. Wallace, and M. A. Valenzuela, "Cogging torque reduction in an axial flux PM machine via stator slot displacement and skewing," *IEEE Trans. Ind. Appl.*, vol. 43, no. 3, pp. 685–693, Jun. 2007.

[43] D. A. Gonzalez, J. A. Tapia, and A. L. Bettancourt, "Design consideration to reduce cogging torque in axial flux permanent-magnet machines," *IEEE Trans. Magn.*, vol. 43, no. 8, pp. 3435–3440, Aug. 2007.

[44] T. Brown, G. Heins, S. Hobbs, M. Thiele, and J. Davey, "Cogging torque prediction for mass-produced axial flux PMSM stators," in *Proc. IEEE IEMDC*, May 2011, pp. 206–211.

[45] D. K. Woo, J. H. Choi, M. Ali, and J. H. Kyo, "A novel multimodal optimization algorithm applied to electromagnetic optimization," *IEEE Trans. Magn.*, vol. 47, no. 6, pp. 1667–1673, Jun. 2011.

[46] G. De Donato, F. G. Capponi, G. A. Rivellini, and F. Caricchi, "Integral-slot versus fractional-slot concentrated-winding axial-flux permanent-magnet machines: Comparative design, FEA, and experimental tests," *IEEE Trans. Ind. Appl.*, vol. 48, no. 5, pp. 1487–1495, Oct. 2012.

[47] A. Boglietti, A. Cavagnino, D. Staton, M. Shanel, M. Mueller, and C. Mejuto, "Evolution and modern approaches for thermal analysis of electrical machines," *IEEE Trans. Ind. Electron.*, vol. 56, no. 3, pp. 871–882, Mar. 2009.

[48] D. A. Howey, P. R. N. Childs, and A. S. Holmes, "Air-gap convection in rotating electrical machines," *IEEE Trans. Ind. Electron.*, vol. 59, no. 3, pp. 1367–1375, Mar. 2012.

[49] H. Sugimoto *et al.*, "Development of an axial flux type PM synchronous motor with the liquid nitrogen cooled HTS armature windings," *IEEE Trans. Appl. Supercond.*, vol. 17, no. 2, pp. 1637–1640, Jun. 2007.

[50] C. H. Lim, G. Airoldi, R. G. Dominy, and K. Mahkamov, "Experimental validation of CFD modelling for heat transfer coefficient predictions in axial flux permanent magnet generators," *Int. J. Thermal Sci.*, vol. 50, no. 12, pp. 2451–2463, 2011.

[51] F. Marignetti, V. D. Colli, and Y. Coia, "Design of axial flux PM synchronous machines through 3-D coupled electromagnetic thermal and fluid-dynamical finite-element analysis," *IEEE Trans. Ind. Electron.*, vol. 55, no. 10, pp. 3591–3601, Oct. 2008.

[52] D. A. Howey, A. S. Holmes, and K. R. Pullen, "Measurement and CFD prediction of heat transfer in air-cooled disc-type electrical machines," *IEEE Trans. Ind. Appl.*, vol. 47, no. 4, pp. 1716–1723, Aug. 2011.

[53] C. H. Lim *et al.*, "2-D lumped-parameter thermal modelling of axial flux permanent magnet generators," in *Proc. 18th ICEM*, 2008, pp. 1–6.

[54] N. Rostami, M. Feyzi, J. Pyrhonen, A. Parviainen, and M. Niemela, "Lumped-parameter thermal model for axial flux permanent magnet machines," *IEEE Trans. Magn.*, vol. 49, no. 3, pp. 1178–1184, Mar. 2013.

[55] G. Airoldi *et al.*, "Computations on heat transfer in axial flux permanent magnet machines," in *Proc. 18th ICEM*, 2008, pp. 1–6.

[56] Y. Chong, D. A. Magahy, J. Chick, M. A. Mueller, D. A. Staton, and A. S. McDonald, "Numerical modelling of an axial flux permanent magnet machine for convection heat transfer," in *Proc. IET Conf. RPG*, Sep. 2011, pp. 1–6.

[57] C. T. Liu, T. S. Chiang, J. F. D. Zamora, and S. C. Lin, "Optimal operational strategy design of a single-sided permanent magnet axial-flux motor for electrical vehicle application," in *Proc. Ind. Appl. Conf. 38th Rec. IAS Annu. Meeting.*, vol. 3. Oct. 2003, pp. 1677–1683.

[58] H. Vansompel, P. Sergeant, and L. Dupre, "Optimized design considering the mass influence of an axial flux permanent-magnet synchronous generator with concentrated pole windings," *IEEE Trans. Magn.*, vol. 46, no. 12, pp. 4101–4107, Dec. 2010.

[59] W. Fei, P. C. K. Luk, and T. S. E. Hasan, "Rotor integrity design for a high-speed modular air-cored axial-flux permanent-magnet generator," *IEEE Trans. Ind. Electron.*, vol. 58, no. 9, pp. 3848–3858, Sep. 2011.

[60] A. Di Gerlando, G. Foglia, M. F. Iacchetti, and R. Perini, "Axial flux PM machines with concentrated armature windings: Design analysis and test validation of wind energy generators," *IEEE Trans. Ind. Electron.*, vol. 58, no. 9, pp. 3795–3805, Sep. 2011.

[61] S. H. Lee, D. J. Kim, J. P. Hong, and J. H. Park, "Characteristic comparison between the spiral and the lamination stator in axial field slotless machines," *IEEE Trans. Magn.*, vol. 45, no. 10, pp. 4547–4549, Oct. 2009.

[62] G. De Donato, F. G. Capponi, and F. Caricchi, "On the use of magnetic wedges in axial flux permanent magnet machines," *IEEE Trans. Ind. Electron.*, vol. 60, no. 11, pp. 4831–4840, Nov. 2013.

[63] G. De Donato, F. G. Capponi, and F. Caricchi, "No-load performance of axial flux permanent magnet machines mounting magnetic wedges," *IEEE Trans. Ind. Electron.*, vol. 59, no. 10, pp. 3768–3779, Oct. 2012.

[64] L. Del Ferraro, F. Caricchi, and F. G. Capponi, "Analysis and comparison of a speed-dependant and a torque-dependant mechanical device for wide constant power speed range in AFPM starter/alternators," *IEEE Trans. Power Electron.*, vol. 21, no. 3, pp. 720–729, May 2006.

[65] F. Giulii Capponi, R. Terrigi, F. Caricchi, and L. Del Ferraro, "Active output voltage regulation for an ironless axial-flux PM automotive alternator with electromechanical flux weakening," *IEEE Trans. Ind. Appl.*, vol. 45, no. 5, pp. 1785–1793, Sep./Oct. 2009.

[66] J. Zhao *et al.*, "Field weakening capability investigation of an axial flux permanent-magnet synchronous machine with radially sliding permanent magnets used for electric vehicles," *J. Appl. Phys.*, vol. 111, no. 7, pp. 07A719-1–07A719-3, 2012.

[67] D. A. González-Lopez, J. A. Tapia, R. Wallace, and A. Valenzuela, "Design and test of an axial flux permanent-magnet machine with field control capability," *IEEE Trans. Magn.*, vol. 44, no. 9, pp. 2168–2173, Sep. 2008.

[68] T. S. Kwon, S. K. Sul, L. Alberti, and N. Bianchi, "Design and control of an axial-flux machine for a wide flux-weakening operation region," *IEEE Trans. Ind. Appl.*, vol. 45, no. 4, pp. 1258–1266, Aug. 2009.

[69] M. Aydin, S. Huang, and T. Lipo, "Design, analysis, and control of a hybrid field-controlled axial-flux permanent-magnet motor," *IEEE Trans. Ind. Electron.*, vol. 57, no. 1, pp. 78–87, Jan. 2010.

[70] L. Ping-Yi and L. Yen-Shin, "Voltage control technique for the extension of DC-link voltage utilization of finite-speed SPMSM drives," *IEEE Trans. Ind. Electron.*, vol. 59, no. 9, pp. 3392–3402, Sep. 2012.

[71] I. Boldea, M. C. Paicu, and G. D. Andreescu, "Active flux concept for motion-sensorless unified AC drives," *IEEE Trans. Power Electron.*, vol. 23, no. 5, pp. 2612–2618, Sep. 2008.

[72] A. H. Isfahani and S. Vaez-Zadeh, "Effects of magnetizing inductance on start-up and synchronization of line-start permanent-magnet synchronous motors," *IEEE Trans. Magn.*, vol. 47, no. 4, pp. 823–829, Apr. 2011.

[73] M. A. Rahman *et al.*, "Advances on single phase line-start high efficiency interior permanent magnet motors," *IEEE Trans. Ind. Electron.*, vol. 59, no. 3, pp. 1333–1345, Mar. 2012.

[74] B. H. Lee, J. P. Hong, and J. H. Lee, "Optimum design criteria for maximum torque and efficiency of a line-start permanent-magnet motor using response surface methodology and finite element method," *IEEE Trans. Magn.*, vol. 48, no. 2, pp. 863–866, Feb. 2012.

[75] P. Guglielmi, B. Boazzo, E. Armando, G. Pellegrino, and A. Vagati, "Permanent magnet minimization in PM assisted synchronous reluctance motor for wide speed range," *IEEE Trans. Ind. Appl.*, vol. 49, no. 1, pp. 31–41, Feb. 2013.

[76] A. Mahmoudi, S. Kahourzade, N. A. Rahim, W. P. Hew, and N. F. Ershad, "Slot-less torus solid-rotor-ringed line-start axial-flux permanent-magnet motor," *Progr. Electromagn. Res.*, vol. 131, pp. 331–355, Nov. 2012.

[77] A. Mahmoudi, S. Kahourzade, N. A. Rahim, and W. P. Hew, "Improvement to performance of solid-rotor-ringed line-start axial-flux permanent-magnet motor," *Progr. Electromagn. Res.*, vol. 124, pp. 383–404, Apr. 2012.

[78] A. Mahmoudi, S. Kahourzade, N. A. Rahim, W. P. Hew, and M. Uddin, "Design, analysis, and prototyping of a novel-structured solid-rotor-ringed line-start axial-flux permanent-magnet motor," *IEEE Trans. Ind. Electron.*, vol. 61, no. 4, pp. 1722–1734, Apr. 2014.

[79] J. F. Eastham, F. Profumo, A. Tenconi, R. H. Cottingham, P. Coles, and G. Gianolio, "Novel axial flux machine for aircraft drive: Design and modeling," *IEEE Trans. Magn.*, vol. 38, no. 5, pp. 3003–3005, Sep. 2002.

[80] A. S. Holmes, H. Hong, and K. R. Pullen, "Axial-flux permanent magnet machines for micropower generation," *J. Microelectromech. Syst.*, vol. 14, no. 1, pp. 54–62, Feb. 2005.

[81] P. J. Masson, M. Breschi, P. Tixador, and C. A. Luongo, "Design of HTS axial flux motor for aircraft propulsion," *IEEE Trans. Appl. Supercond.*, vol. 17, no. 2, pp. 1533–1536, Jun. 2007.

[82] S. M. A. Sharkh and M. T. N. Mohammad, "Axial field permanent magnet DC motor with powder iron armature," *IEEE Trans. Energy Convers.*, vol. 22, no. 3, pp. 608–613, Sep. 2007.

[83] D. Kowal, P. Sergeant, L. Dupre, and A. V. Bossche, "Comparison of nonoriented and grain-oriented material in an axial flux permanent-magnet machine," *IEEE Trans. Magn.*, vol. 46, no. 2, pp. 279–285, Feb. 2010.

[84] F. Marignetti, V. D. Colli, and S. Carbone, "Comparison of axial flux PM synchronous machines with different rotor back cores," *IEEE Trans. Magn.*, vol. 46, no. 2, pp. 598–601, Feb. 2010.

[85] Z. Wang *et al.*, "Development of an axial gap motor with amorphous metal cores," *IEEE Trans. Ind. Appl.*, vol. 47, no. 3, pp. 1293–1299, Jun. 2011.

[86] H. Jagau, M. A. Khan, and P. S. Barendse, "Design of a sustainable wind generator system using redundant materials," in *Proc. IEEE ECCE*, Sep. 2011, pp. 1628–1635.

[87] T. F. Chan, W. Wang, and L. L. Lai, "Magnetic field in a transverse- and axial-flux permanent magnet synchronous generator from 3-D FEA," *IEEE Trans. Magn.*, vol. 48, no. 2, pp. 1055–1058, Feb. 2012.

[88] L. Hao, M. Lin, X. Zhao, X. Fu, Z. Q. Zhu, and P. Jin, "Static characteristics analysis and experimental study of a novel axial field flux-switching permanent magnet generator," *IEEE Trans. Magn.*, vol. 48, no. 11, pp. 4212–4215, Nov. 2012.

[89] W. Wang, K. W. E. Cheng, K. Ding, and L. C. Meng, "A novel approach to the analysis of the axial-flux permanent-magnet generator with coreless stator supplying a rectifier load," *IEEE Trans. Magn.*, vol. 47, no. 10, pp. 2391–2394, Oct. 2011.

[90] S. Brisset, D. Vizireanu, and P. Brochet, "Design and optimization of a nine-phase axial-flux PM synchronous generator with concentrated winding for direct-drive wind turbine," *IEEE Trans. Ind. Appl.*, vol. 44, no. 3, pp. 707–715, Jun. 2008.

[91] J. Y. Lee, D. H. Koo, S. R. Moon, and C. K. Han, "Design of an axial flux permanent magnet generator for a portable hand crank generating system," *IEEE Trans. Magn.*, vol. 48, no. 11, pp. 2977–2980, Nov. 2012.

[92] S. C. Oh and A. Emadi, "Test and simulation of axial flux-motor characteristics for hybrid electric vehicles," *IEEE Trans. Veh. Technol.*, vol. 53, no. 3, pp. 912–919, May 2004.

[93] K. Rahman, N. Patel, T. Ward, J. Nagashima, F. Caricchi, and F. Crescimbini, "Application of direct-drive wheel motor for fuel cell electric and hybrid electric vehicle propulsion system," *IEEE Trans. Ind. Appl.*, vol. 42, no. 5, pp. 1185–1192, Oct. 2006.

[94] Y. P. Yang and D. S. Chuang, "Optimal design and control of a wheel motor for electric passenger cars," *IEEE Trans. Magn.*, vol. 43, no. 1, pp. 51–61, Jan. 2007.

[95] T. D. Nguyen, K. J. Tseng, S. Zhang, and H. T. Nguyen, "A novel axial flux permanent-magnet machine for flywheel energy storage system: Design and analysis," *IEEE Trans. Ind. Electron.*, vol. 58, no. 9, pp. 3784–3794, Sep. 2011.

[96] F. Caricchi, F. Crescimbini, and O. Honrati, "Modular axial-flux permanent-magnet motor for ship propulsion drives," *IEEE Trans. Energy Convers.*, vol. 14, no. 3, pp. 673–679, Sep. 1999.

[97] R. L. Ficheux, F. Caricchi, F. Crescimbini, and O. Honorati, "Axial-flux permanent-magnet motor for direct-drive elevator systems without machine room," *IEEE Trans. Ind. Appl.*, vol. 37, no. 6, pp. 1693–1701, Dec. 2001.

[98] M. C. Tsai and L. Y. Hsu, "Design of a miniature axial-flux spindle motor with rhomboidal PCB winding," *IEEE Trans. Magn.*, vol. 42, no. 10, pp. 3488–3490, Oct. 2006.

[99] H. Raisigel, O. Cugat, and J. Delamare, "Permanent magnet planar micro-generators," *Sens. Actuators A, Phys.*, vol. 130, pp. 438–444, Aug. 2006.

[100] F. Caricchi, F. Maradei, G. De Donato, and F. G. Capponi, "Axial-flux permanent-magnet generator for induction heating gensets," *IEEE Trans. Ind. Electron.*, vol. 57, no. 1, pp. 128–137, Jan. 2010.

[101] R. Cuzner, D. Drews, W. Kranz, A. Bendre, and G. Venkataraman, "Power dense, shipboard compatible low horsepower variable frequency drives," *IEEE Trans. Ind. Appl.*, vol. 48, no. 6, pp. 2121–2128, Dec. 2012.

[102] Z. Kohari, Z. Nadudvari, L. Szlama, M. Keresztesi, and I. Csaki, "Test results of a compact disk-type motor/generator unit with superconducting bearings for flywheel energy storage systems with ultra-low idling losses," *IEEE Trans. Appl. Supercond.*, vol. 21, no. 3, pp. 1497–1501, Jun. 2011.

[103] F. Herrault, D. P. Arnold, I. Zana, P. Galle, and M. G. Allen, "High temperature operation of multi-watt, axial-flux, permanent-magnet microgenerators," *Sens. Actuators A, Phys.*, vol. 148, no. 1, pp. 299–305, 2008.

[104] F. G. Capponi, R. Terrigi, F. Caricchi, and L. D. Ferraro, "Active output voltage regulation for an ironless axial-flux pm automotive alternator with electromechanical flux weakening," *IEEE Trans. Ind. Appl.*, vol. 45, no. 5, pp. 1785–1793, Oct. 2009.

[105] K. Lee *et al.*, "Micro-energy storage system using permanent magnet and high-temperature superconductor," *Sens. Actuators A, Phys.*, vol. 143, no. 1, pp. 106–112, 2008.

[106] K. Sitapati and R. Krishnan, "Performance comparisons of radial and axial field, permanent-magnet, brushless machines," *IEEE Trans. Ind. Appl.*, vol. 37, no. 5, pp. 1219–1226, Sep./Oct. 2001.

[107] A. Cavagnino, M. Lazzari, F. Profumo, and A. Tenconi, "A comparison between the axial flux and the radial flux structures for PM synchronous motors," *IEEE Trans. Ind. Appl.*, vol. 38, no. 6, pp. 1517–1524, Nov./Dec. 2002.
[108] A. Chen, R. Nilssen, and A. Nysveen, "Performance comparisons among radial-flux, multistage axial-flux and three-phase transverse-flux PM machines for downhole applications," *IEEE Trans. Ind. Appl.*, vol. 46, no. 2, pp. 779–789, Mar./Apr. 2010.
[109] J. Pippuri, A. Manninen, J. Keränen, and K. Tammi, "Torque density of radial, axial and transverse flux permanent magnet machine topologies," *IEEE Trans. Magn.*, vol. 49, no. 5, pp. 2339–2342, May 2013.
[110] R. Qu, M. Aydin, and T. A. Lipo, "Performance comparison of dual-rotor radial-flux and axial-flux permanent-magnet BLDC machines," in *Proc. IEEE IEMDC*, Jun. 2003, pp. 1948–1954.

Solmaz Kahourzade (S'92) was born in Bandar Abbas, Iran, in 1984. She received the B.S. degree in electronic engineering from the K. N. Toosi University of Technology, Tehran, Iran, and the M.Eng. degree in electrical power engineering from the University of Malaya, Kuala Lumpur, Malaysia, in 2007 and 2012, respectively.

She is currently a Research Assistant with the UM Power Energy Dedicated Advanced Centre, Kuala Lumpur. She is the author and coauthor of more than 20 papers in international journals and conferences.

Amin Mahmoudi (S'11–M'13) was born in Bandar Abbas, Iran, in 1983. He received the B.S. degree in electrical engineering from Shiraz University, Shiraz, Iran, the M.S. degree in electrical power engineering from the Amirkabir University of Technology, Tehran, Iran, and the Ph.D. degree from the University of Malaya, Kuala Lumpur, Malaysia, in 2005, 2008, and 2013, respectively.

His current research interests include the modeling and design of electrical machinery.

Dr. Mahmoudi is a member of the Institution of Engineering and Technology and a Chartered Engineer. He is also a member of the Engineers Australia.

Hew Wooi Ping (M'11) was born in Kuala Lumpur, Malaysia, in 1957. He received the bachelor's and master's degrees in electrical engineering from the University of Technology, Johor Bahru, Malaysia, in 1981, and the Ph.D. degree from the University of Malaya, Kuala Lumpur, Malaysia, in 2000.

He is a Professor with the University of Malaya and a Chartered Engineer. His current research interests include electrical drives, electrical machine design, application of fuzzy logic/neural network to electrical-machine-related applications, and renewable energy (solar and wind).

Dr. Ping is a member of IET.

Mohammad Nasir Uddin (S'99–M'00–SM'04) received the B.Sc. and M.Sc. degrees in electrical and electronic engineering from the Bangladesh University of Engineering and Technology, Dhaka, Bangladesh, 1993 and 1996, respectively, and the Ph.D. degree in electrical engineering from the Memorial University of Newfoundland, St. John's, NL, Canada, in 2000.

He is currently a Professor with the Department of Electrical Engineering, Lakehead University, Thunder Bay, ON, Canada. His current research interests include power electronics, electric motor drives, and the application of intelligent controllers.

Dr. Uddin is serving as a Chair of the IEEE IAS Industrial Automation and Control Committee (IACC). He is the Technical Chair for the IEEE IAS (IACC) Annual Meetings 2011 and 2012. Previously, he was the Transactions Review Chair for the IEEE/IAS/IACC. Recently, he was bestowed upon with the prestigious Lakehead University Distinguished Researcher Award in 2010. He is the recipient of two First Prize and one Third Prize Paper Awards from the IEEE/IAS/IACC Committee, and both 2004 Contributions to Research Award and Contributions to Teaching Award from LU. He is a registered Professional Engineer in the Province of Ontario, Canada.